Journal of ELECTRONIC MATERIALS, Vol. 43, No. 4, 2014
DOI: 10.1007/s11664-014-3025-5

Cobalt–Polymer Nanocomposite Dielectrics for Miniaturized Antennas

P. MARKONDEYA RAJ,[1,3] HIMANI SHARMA,[1] G. PRASHANT REDDY,[1] NEVIN ALTUNYURT,[1] MADHAVAN SWAMINATHAN,[1] RAO TUMMALA,[1] and VIJAY NAIR[2]

1.—Packaging Research Center, Georgia Institute of Technology, Atlanta, GA 30332-0560, USA. 2.—Intel Corporation, 5000 W. Chandler Boulevard, Chandler, AZ 85226, USA. 3.—e-mail: raj@ece.gatech.edu

Cobalt–polymer magnetic nanocomposites have been synthesized and characterized for their microstructure and properties such as permeability, permittivity, dielectric and magnetic losses from 100 MHz to 2 GHz to study their suitability as antenna dielectrics. Oxide-passivated cobalt nanoparticles were dispersed in epoxies to form nanocomposite toroids and thin-film resonator structures on organic substrates. Permeabilities of 2.10 and 2.65 were measured up to 500 MHz, respectively, with 25-nm to 50-nm and 5-nm nanoparticles in the nanocomposites. The loss tangent ranged from 0.02 to 0.04 at these frequencies. A combination of stable permeability of ~2 at 1 GHz to 2 GHz and permittivity of ~7 was achieved with nanocomposites having 5-nm nanoparticles. The magnetic nanomaterials described in this paper can overcome the limitations from domain-wall and eddy-current losses in microscale metal–polymer composites, leading to enhanced frequency stability. The paper also demonstrates integration of metal–polymer nanocomposites as thin-film build-up layers with two-metal-layer structures on organic substrates.

Key words: Antenna, nanocomposites, substrates, integration, magnetodielectrics, magnetic loss

INTRODUCTION

Current and emerging radiofrequency (RF) subsystems need materials and structures with higher permittivity and permeability along with frequency and thermal stability, and low loss. These properties are critical for component and system performance enhancement, system integration, and miniaturization.[1] Existing RF materials such as low-temperature cofired ceramics (LTCCs) and polymer dielectrics show fundamental limitations in terms of component miniaturization because of their inferior properties such as low permittivity and absence of magnetic properties. Enhancement in permittivity or permeability usually comes at the expense of dielectric loss, and temperature and frequency dependence of properties, which makes them unsuitable for use in high-performance RF components.[2] Amongst the RF components, the antenna is still considered a major barrier to system miniaturization because the performance of an antenna is directly dependent on its physical size.[3] To decrease the size of an antenna, it has to be surrounded by a material with either high permittivity (ε) or permeability (μ), which would shorten the wavelength by a factor of $1/\sqrt{\varepsilon\mu}$[4,5] and lead to miniaturized designs. Over the past decade, the materials employed in high-frequency planar antennas were mostly limited to thick-film LTCCs[6,7] owing to their low loss, stable properties, and partial integration capability, although end-systems made using these technologies are still bulky and costly. Polymer dielectrics, on the other hand, provide the benefits of low-cost manufacturing and total integration capabilities with other polymer-based systems. However, traditional organic materials such as epoxies have high electrical losses at high frequencies, while

(Received September 4, 2013; accepted January 9, 2014; published online February 8, 2014)

low-loss organics based on fluoropolymers, benzocyclobutene (BCB), and others have low permittivity and no magnetic properties. These limitations lead to large component designs, and also make it extremely difficult to build integrated high-performance front-end modules.[8,9]

Magnetic films provide unique opportunities to address the fundamental limitations of traditional RF dielectrics. In addition to enhancing the inductance density through higher permeability, magnetic films can also potentially lead to a dramatic reduction in antenna size because of their combined effect of high permittivity and permeability. Compared with traditional polymer dielectrics, increases in the permeability and permittivity by fourfold in magnetic nanocomposites can reduce antenna dimensions by a factor of four, resulting in significant antenna miniaturization. By tuning the formulation, materials can be designed to have lower permittivity-to-permeability ratio to achieve good impedance matching with that of free space.[10] The antenna bandwidth on such magnetic substrates will therefore be wider than that with high-permittivity dielectric substrates[11–13] that provide the same miniaturization from the permittivity alone. The high permeability suppresses backscattering and improves the radiation efficiency, resulting in further performance enhancement.[2] Magnetic materials have been widely studied at frequencies above 100 MHz. They are classified into ferrites, microscale metal composites, nanoscale metal composites, and anisotropic composite structures and are briefly reviewed here in these categories.

Compounds of ferrites and other oxides are widely used for microwave applications such as circulators, isolators, and phase-shifters because of their higher resistivity resulting in lower eddy-current losses and frequency stability.[14] Recent study showed stable properties in nanocomposites containing ferrite nanoparticles, with permeabilities of 5 to 10 up to 15 GHz.[15] Compounds based on BaO, Fe_2O_3, and other oxides (MO, M = Co, Ni, etc.) with hexagonal structures are more suited for high-frequency applications.[16] When Co is the other oxide used along with BaO and Fe_2O_3, they are classified as Co_2M (barium hexaferrite, $BaFe_{12}O_{19}$), Co_2Y ($Ba_2Co_2Fe_{12}O_{22}$), or Co_2Z (mixtures of M and Y, $Ba_3Co_2Fe_{12}O_{41}$). Recently, hexaferrites and their nanocomposites with glass and polymer were characterized for antennas.[17–19] Co_2Z hexaferrites showed permeability of above 10 at 300 MHz to 400 MHz.[19] Permeability of ~2 with loss of 0.03 has been shown for ferrite–glass nanocomposites with frequency stability of up to 2 GHz to 3 GHz.[18]

Traditional metal-based magnetic composites at submicro- or microscale also do not show adequate frequency stability and low loss. The eddy-current losses are directly proportional to the particle size and are therefore higher for microscale particles[20] compared with nanoparticles. Larger particles also have multiple domains which generate additional losses due to domain-wall resonance.[21] Several studies on magnetic metal–polymer composites have been reported, particularly focusing on the iron–polymer and NiFe–polymer systems.[22–25] With large, microsized particles, permeabilities of above 100 are reported. These particles show lower coercivity and higher intrinsic permeability. However, the magnetic losses become significant even at 1 MHz.

The frequency stability of microscale composites can be enhanced with anisotropic structures. Studies on NiFe alloy flake–polymer nanocomposites showed permeabilities of 5 to 10 with losses of above 0.1 at 1 GHz.[26] In another study by Yang et al.,[27] oriented flake-shaped Fe alloy particles mixed in a paraffin matrix showed permeability of 8 at 100 MHz and 3.9 up to 2 GHz. Oriented ferrite films with hard axis in the direction perpendicular to the film plane have also been shown to have enhanced frequency stability.[28]

Magnetic materials that comprise nanoscale metal particles in an amorphous matrix provide unique opportunities to address the fundamental limitations of microscale magnetic materials. Higher permeability and frequency stability can be achieved in magnetic nanocomposites by reducing the particle size and the separation between neighboring metal particles down to the nanoscale, which leads to magnetic exchange coupling phenomena;[29,30] For example, Co- or Fe-based nanocomposites show much higher permeability and frequency stability at microwave frequencies than those obtained from bulk Co or Fe metal or their microscale composites.[31] The exchange coupling interaction, which leads to magnetic ordering within a grain, extends out to the neighboring environments within a characteristic distance, l_{ex}, which is ~20 nm for Fe or Co.[32,33] The exchange interaction in nanocomposites also leads to cancelation of the magnetic anisotropy of individual particles and the demagnetizing effect, leading to higher permeability and lower coercivity.[34] Because of the nanosized metal particles, the eddy currents produced within the particles are also negligibly small, leading to much lower loss for nanocomposites, compared with conventional microsized ferrites or powder materials. These nanomagnetic structures with high permeability were mostly obtained through sputtering, which cannot yield the thick magnetic films required for antenna applications. Nanoparticle composites in polymer matrices synthesized via chemical synthesis routes can accomplish this. However, they do not show such high permeability as sputtered films, although they have improved frequency stability and lower loss compared with their microstructured counterparts.[28,33,35–39] Anisotropic one-dimensional nanostructures based on nickel or cobalt nanowires or filaments have been studied to overcome the limitations of isotropic nanocomposites. Nanowire

Table I. Selected references on magnetodielectrics and their electromagnetic properties at microwave frequencies

Material	Structure	Properties	Frequency	Ref.
Passivated metal nanoparticles (NiFe)	~100-nm particles	Permeability: 12	1 GHz	38
Oxide-passivated iron and nickel nanocomposites	~100-nm particles	Permeability: 1.3 to 1.5 Permittivity: 14 to 15 Magnetic loss: 0.2 to 0.3	2 GHz to 18 GHz	42
Co_2Z–glass nanocomposites	~100-nm grains	Permeability: 2 Magnetic loss: 0.02 Permittivity: 7 Dielectric loss: 0.01	2 GHz to 3 GHz	18
Spinel–wax nanocomposites	60-nm particles	Permeability: 4 to 9 Permittivity: 3 to 8 Magnetic loss: 0.2	9 GHz to 15 GHz	15
Co_2Z ferrites, sintered ceramic films	10-μm sintered grains	Permeability: 9 to 10 Permittivity: 9 to 10	100 MHz to 400 MHz	19
$Ni_xZn_xFe_2O_4$, sputtered ferrite films	Crystallite size: 10 nm to 15 nm Thickness: 1.5 μm	Permeability: 7	1 GHz	28
Oriented metal flakes (iron)	Thickness: 100 nm Size: 5 μm Grain size: 13 nm	Permeability: 3 to 6 Magnetic loss: 3	2 GHz to 3 GHz	27
Magnetic nanowire array approach (cobalt)	Cobalt nanowires 50-nm pores 90-nm interpore distance	Permeability: 3.5 Magnetic loss: 0.045	4.5 GHz	40

composites with crystallographically oriented cobalt of high magnetocrystalline field anisotropy showed permeability of 3.5 and loss of 0.045 up to 4.5 GHz.[40,41] A brief summary of the microwave properties of magnetodielectrics is provided in Table I.

Polymer nanocomposites loaded with metal nanoparticles also show enhancement in permittivity with higher metal-filler content. The additional polarization, which is strongly frequency dependent, occurs because of charge redistribution at metal–polymer interfaces that creates electric dipoles. Permittivities of ~10 are typically seen in metal–polymer nanocomposites in the 1 GHz to 5 GHz range with oxide-passivated nanoscale particles.[42] Several models have been proposed in the literature to explain the dielectric properties of metal–polymer nanocomposites.[43–45] The models suggest that the particle conductivity, size, and permittivity of the medium surrounding the nanoparticles influence the dielectric relaxation frequency. Beyond the relaxation frequency, the permittivity of the nanocomposite approaches that of the matrix.

Although several reports are available on the microwave properties of metal nanocomposites,[33–39] integration of magnetic nanocomposites as thin (20 μm to 100 μm) films on an organic substrate for low-cost microwave applications, and their characterization by probing planar inductive and capacitive structures to study magnetic and dielectric properties simultaneously, have not been reported. Such integration using standard package fabrication technologies and high-frequency characterization of magnetic polymer nanocomposite films are critical to understand their applicability for low-cost organic packaging. This paper thus investigates the processing and properties of novel magnetic nanocomposites for their magnetic permeability, dielectric constant, and dielectric loss up to 2 GHz. Based on these measurements, the suitability of these materials for high-frequency antenna applications is assessed.

EXPERIMENTAL PROCEDURES

Commercially available cobalt nanoparticles (Strem Chemicals, Inc., Newburyport, MA, USA), synthesized by carbonyl decomposition and passivated with a layer of sodium dioctylsulfosuccinate (AOT) surfactant to protect the surfaces, were used. The AOT coating, in conjunction with the native oxide, prevents oxidation during initial handling.

Polymer Matrix Selection

Epoxies were used as the polymer matrices on organic substrates because of their process compatibility with standard package fabrication. AOT-coated 5-nm cobalt nanoparticles were directly mixed and milled with the monomer solution. The oxide-passivated cobalt nanoparticles, on the other hand, were first milled in a solvent (propylene glycol methyl ether acetate, PGMEA; CAS no. 108-65-6) medium. This process results in the disintegration of aggregates to obtain finely dispersed spherical Co nanopowder in PGMEA. Epoxy resin (EPON828™; Momentive Performance Materials, USA) was added to this suspension and again milled for 6 h, followed by addition of curing agent (EPIKURE 3300; Momentive Performance Materials, USA) and final mixing for 2 h.

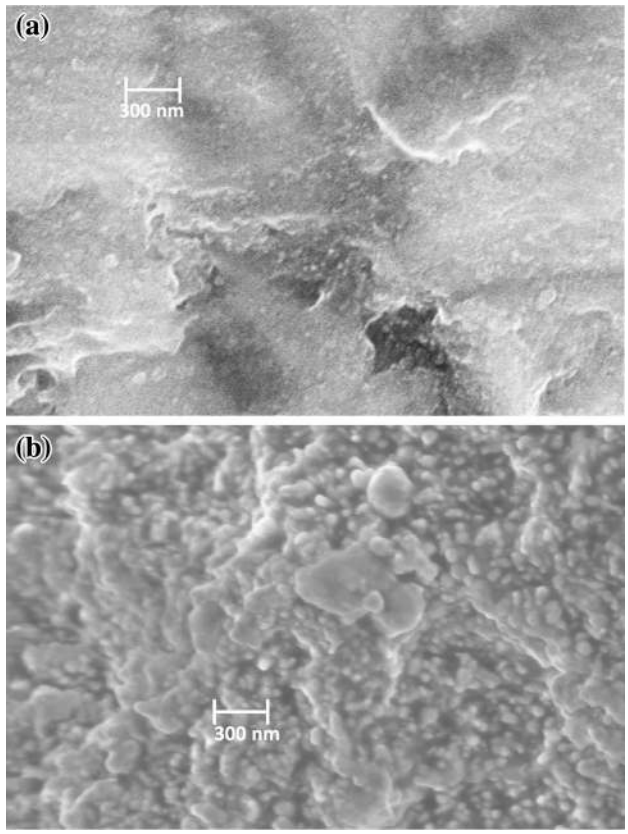

Fig. 1. SEM images of (a) 5-nm and (b) 25-nm Co–epoxy nanocomposites.

Scanning electron micrography (SEM) images for the two nanocomposite systems are shown in Fig. 1a, b. The nanocomposite with 5-nm particles showed well-dispersed particles, while the other system with 25-nm nanoparticles showed larger features of 100 nm, indicating some particle aggregation. To fabricate the toroid test structures, dried metal–polymer composite was crushed and dry-pressed in a steel mold, followed by curing the polymer. Magnetization (B)–field (H) loops were obtained by using a vibrating-sample magnetometer (VSM, 736 series; Lakeshore). Measurements up to 500 MHz were performed using an impedance analyzer (4291B; Agilent).

Fabrication of Thin-Film Characterization Test Structures

To fabricate thin-film structures by screen-printing, the suspension was converted to a high-viscosity paste

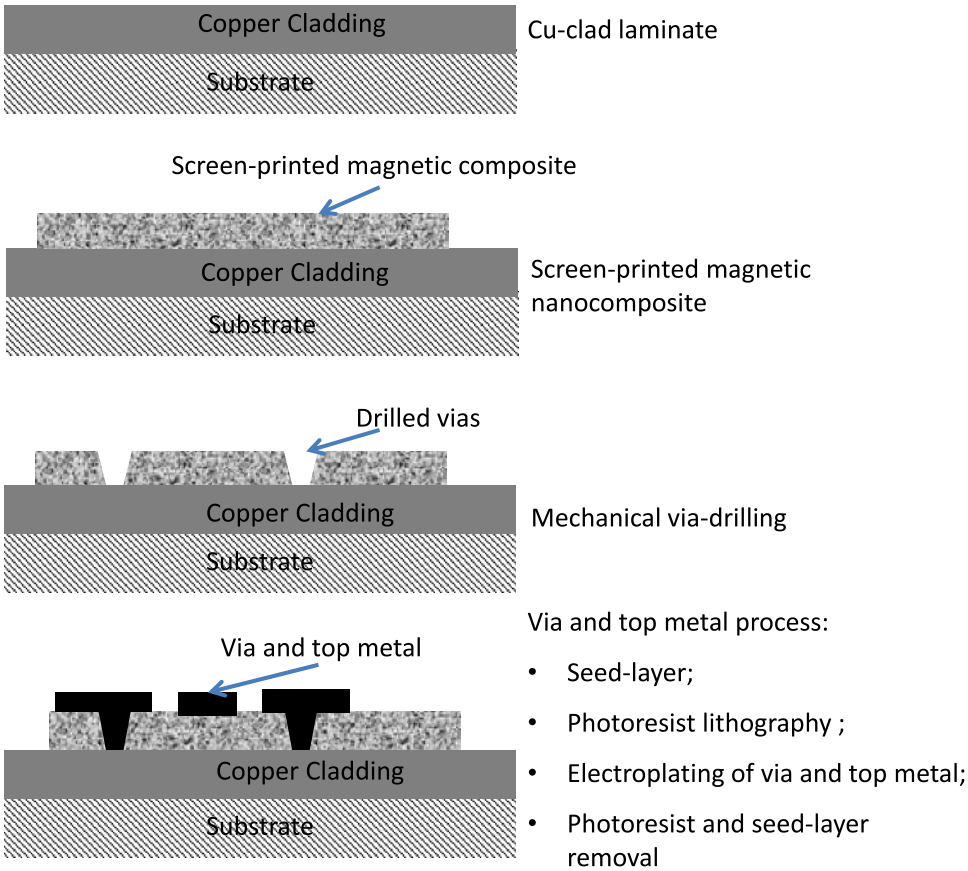

Fig. 2. Process flow for test-vehicle fabrication of high-frequency characterization structures.

by heating it in a nitrogen-flow oven to slowly evaporate the solvent. Cu-cladded FR-4 (flame-retardant) laminates were used as the substrates for fabricating the test structures. The laminate consisted of 18-μm copper cladding on a glass–polymer composite, usually referred to as FR-4. The polymer consists of epoxy with flame retardants and other additives to increase the glass-transition temperature and lower the coefficient of thermal expansion (CTE). Traditional processes that are compatible with existing infrastructure such as screen-printing, mechanical via-drilling, and wet metallization using electroplated copper were employed. With thicker vias and higher solid loading, screen-printing did not give good process control. Hence, stencil-printing followed by mechanical drilling of vias (Quick Circuit 7000; T-Tech, Inc., Norcross, GA) was used in such cases. Drill bits of 0.5 mm (Megatool; Drill Technology, Ada, MI) were utilized for drilling the vias. The top metal layer was formed through a semiadditive process constituting seed-layer deposition, photoresist patterning, and plating, followed by photoresist and seed-layer removal. These process steps are described in Fig. 2.

Optical micrographs of the test vehicles with mechanically drilled vias and electroplated resonator test structures are shown in Fig. 3a. The structure is composed of two metal layers separated by the nanocomposite dielectric. As seen in Fig. 3b, the top metal is framed with another metal layer, which is shorted to the bottom metal with a series of vias with diameter of 0.5 mm. The gap between the framing metal and the top metal is 0.1 mm, and the width, w, of the framing metal is 0.7 mm. The electric wall, created by the series of vias that short the frame to metal, transforms the parallel-plate resonator into a box resonator, created by organic substrate technology. The response of the resonator can be measured using ground–signal–ground (GSG) air probes. The structure is excited by probing it at the corners, such that the signal tip of the probe lands on the top metal while the ground tips land on the frame. In the case of magnetodielectric substrates, however, a parallel-plate resonator is useful only in the frequency range up to the first antiresonance in the transmission impedance response, Z_{12}. In this frequency range, because of the inherent capacitive behavior of the parallel-plate resonator, the impedance response is more sensitive to changes in permittivity, making it possible to characterize the dielectric properties almost independently of the magnetic properties. Therefore, the frequency-dependent data can be extracted by starting with an approximate value for permittivity and by fitting the simulated $\mathrm{Im}(Z_{12})$ and $\mathrm{Re}(Z_{12})$ values to the

measured values to extract the relative permittivity and dielectric loss, respectively.

Similar to the idea of using the inherently capacitive behavior of parallel-plate resonators to characterize the permittivity, structures with inductive impedance response can be used to characterize the permeability. Strip inductors obtained by shorted microstrip lines were used to measure the inductive impedance response. The characterization process starts with vector network analyzer (VNA, 8720ES; Agilent) *s*-parameter measurements and thickness data, followed by curve-fitting of the simulated Z_{11} data to the measured Z_{11} (self-impedance) data. The relative permeability and magnetic loss tangent were used to fit the imaginary and real parts of the simulated data to the measured data.

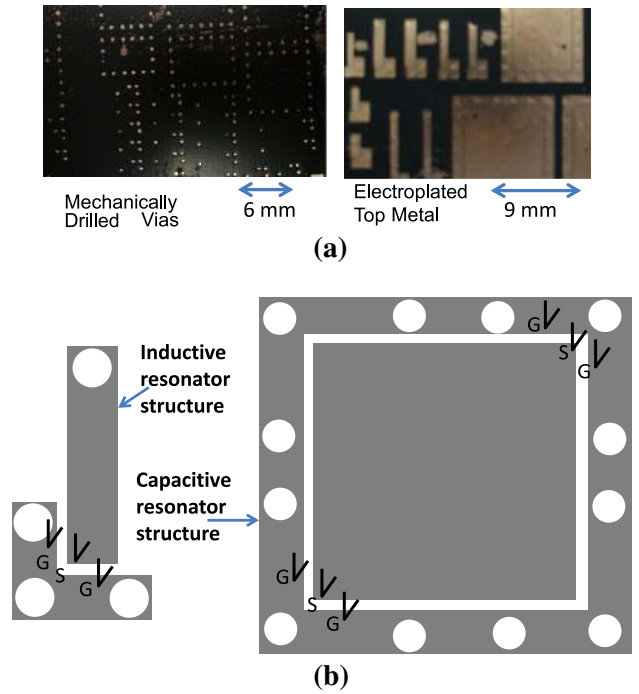

Fig. 3. (a) Optical micrographs of the fabricated test structures: mechanically drilled vias (left), and plated capacitive and inductive resonator structures (right). (b) Schematic test structures with GSG probe locations for exciting the capacitive and inductive resonators; white circles indicate via positions.

RESULTS AND DISCUSSION

The fabricated films were characterized by x-ray diffraction (XRD) analysis to confirm the presence of the crystallographic metal phase. Films with 25-nm particles showed stronger face-centered cubic (FCC) cobalt phase (Fig. 4). The finer (5-nm) nanoparticles showed weak peaks, as suggested by the manufacturer's data. The low saturation magnetization (M_s) and weak peaks indicate the presence of a significant volume of cobalt oxide on the surface, although these are referred to as cobalt–polymer nanocomposites hereinafter.

The cobalt–polymer (5-nm particles) toroids showed stable permeability, as shown in Fig. 5. Permeability of 2.6 to 2.65 was measured in the frequency range of 70 MHz to 500 MHz with steady loss of 0.03 to 0.04. Nanocomposites with 25-nm particles showed permeability of 2.15 to 2.25 in the same frequency range. However, the magnetic loss systematically increased from 0.01 to 0.02, although still being less than the dielectric loss of traditional epoxies. The *B–H* curves obtained from VSM measurements are shown in Fig. 6. The M_s for the nanocomposites with 25-nm nanoparticles was 60 emu/g, while that for the 5-nm nanocomposites was 25.2 emu/g. In spite of having the same metal content, the M_s is different because of the higher oxide fraction for the finer nanoparticles. The key

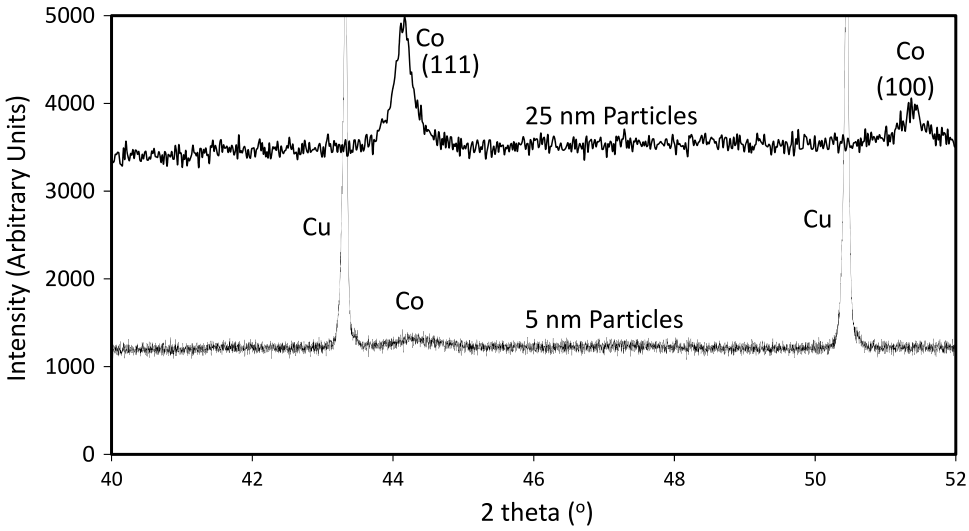

Fig. 4. XRD patterns from the two nanocomposite systems in this study. The 5-nm cobalt nanocomposite films are deposited on copper-clad laminates.

properties are summarized in Table II. The theoretical M_s value of cobalt is 160 emu/g. For 80 wt.% nanoparticle loading in the nanocomposites, the theoretical M_s is 128 emu/g. This indicates that 50 wt.% (for the 5-nm system) and 80 wt.% (for the 25-nm system) of the nanoparticles consist of oxide.

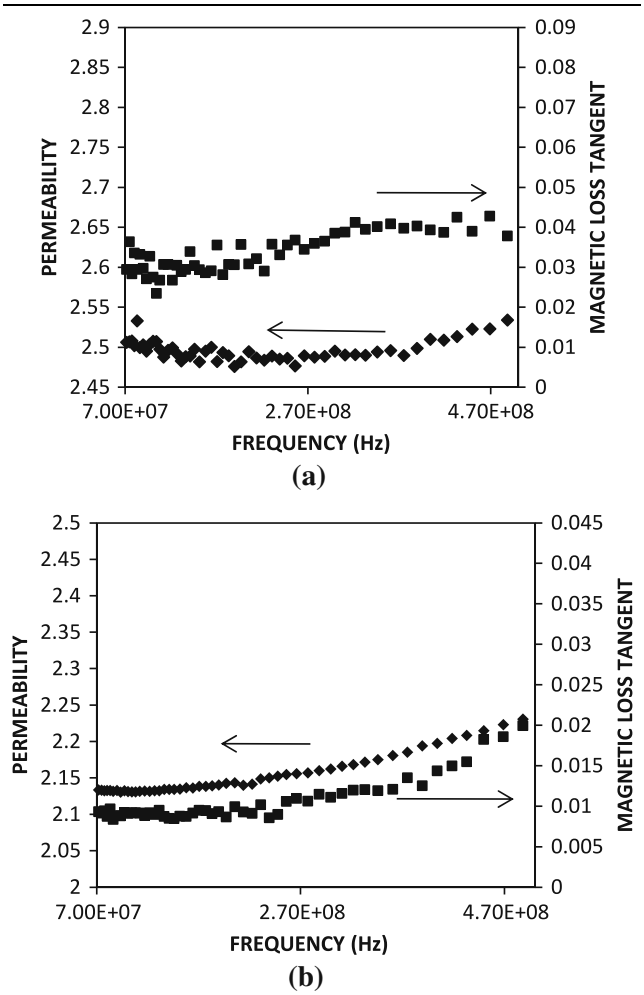

Fig. 5. Permeability versus frequency plots of cobalt–polymer nanocomposites: (a) 5-nm particles and (b) 25-nm to 50-nm particles.

The oxide content is also evident from x-ray photoelectron spectroscopy (XPS) studies (data not reported here) showing strong shoulder peaks corresponding to cobalt in the +2 and +3 oxidation states.

Both curves show high remanence (18.4 emu/g for 25-nm particles, 5.4 emu/g for 5-nm particles) and coercivity (648 Oe for 25-nm particles, 115 Oe for 5-nm particles) compared with traditional soft magnets. When the particle size is small enough to form single domains, the coercivity of nanoparticles is controlled by the magnetic anisotropies and surface effects arising from distortion in the symmetry fields at the surface.[32,46,47] The coercivity is further aggravated in oxide-passivated nanoparticles because of various surface anisotropies such as ferromagnetic–antiferromagnetic exchange anisotropy at CoO–Co interfaces, as described by Berkowitz and Takano.[48]

The relatively stable permeability with 5-nm particles is attributed to the finer size and lower coercivity that resulted in suppressed eddy-current and hysteresis losses. Based on the stable loss properties, 5-nm cobalt nanoparticles were chosen for high-frequency characterization. The inductor and parallel-plate resonators were modeled in Sonnet with the test-vehicle electrode and dielectric geometries in order to accurately model the losses. Characterization was performed up to 2 GHz, beyond which the resonance frequency of the inductor affects the measurements. Characterization of high-frequency magnetic properties was performed by matching the simulated impedance data from Sonnet to the measured impedance data at every frequency point to within 1% accuracy. Sensitivity analysis showed that the permittivity, permeability, and loss tangents converge to ~1% for this level of impedance matching. The characterized values for the relative permeability and magnetic loss tangent are shown in Fig. 7a. The cobalt–polymer nanocomposite with 5-nm Co particle size showed a μ_r of 1.95 ± 0.05. Similarly, Fig. 7b shows the extracted values for the relative permittivity and dielectric loss tangent. As seen in this figure, the relative permittivity is constant at 7.4 ± 0.2 and the

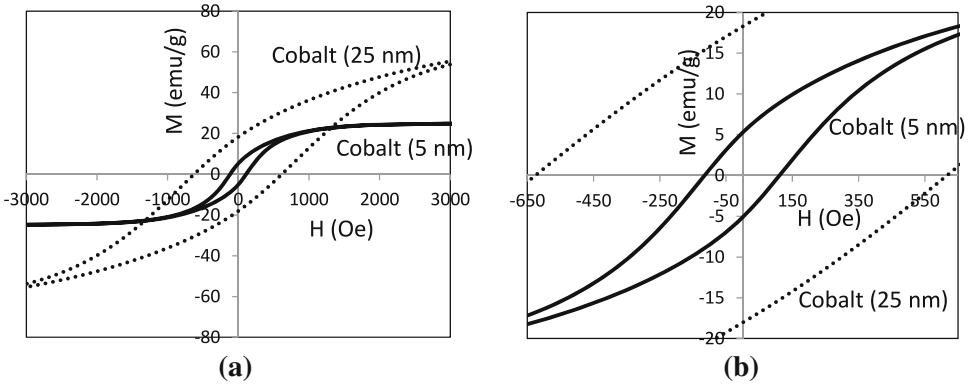

Fig. 6. *B–H* curves for the 5-nm and 25-nm cobalt–polymer nanocomposites from VSM measurements. Panel (b) is a zoomed version of (a).

Table II. Magnetic properties of the nanocomposites

Cobalt–Polymer Nanocomposite	Estimated M_s (emu/g)	Measured M_s (emu/g)	Coercivity (Oe)	Remanence (emu/g)	Permeability	Magnetic Loss
5 nm	128	25.2	115	5.4	2.5–2.55	0.03–0.04
25 nm	128	60	648	18.4	2.15–2.25	0.01–0.02

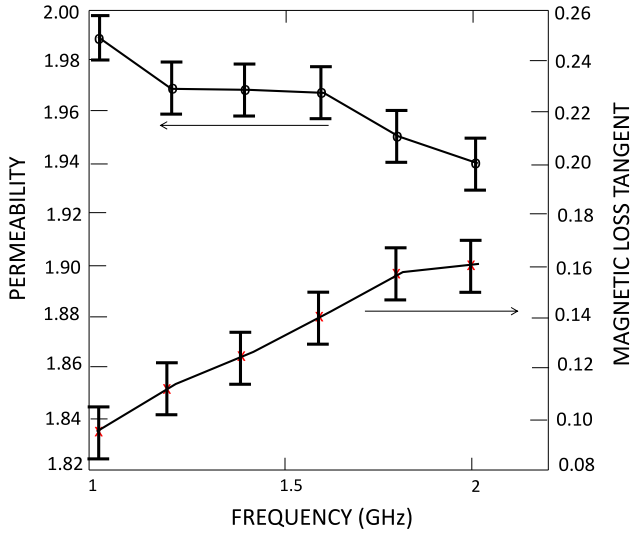

(a)

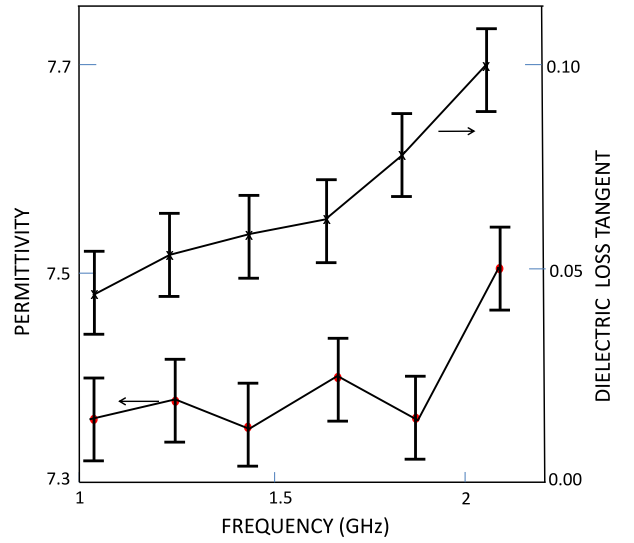

(b)

Fig. 7. Relative permeability (a) and permittivity (b), and the corresponding loss tangents, as a function of frequency for the 5-nm cobalt–polymer nanocomposites.

dielectric loss increases with frequency. The deviation from one sample to another was within 5% and was attributed to local thickness nonuniformity within the device from the paste-printing process. In one-port measurements with inductive resonator structures, network analyzer probes add significant parasitics. Hence, the magnetic loss tangent is expected to have an additional source of error.

High permeability in magnetic nanocomposites usually results from superexchange coupling between nanoparticles. The relatively lower permeability values in the current nanocomposites indicate that such interparticle interactions are weak because of the increased separation between the particles from the relatively lower metal particle loading in the polymer matrix and their packing

density. The processing steps such as ball-milling and curing during polymer composite processing result in significant oxide growth, which suppresses interparticle exchange coupling. The isolated particles retain substantial demagnetization, high coercivity from the metal-oxide exchange anisotropy,[48] and poor interparticle coupling. The high losses of 0.1 at 1 GHz to 2 GHz are attributed to the high coercivity from the single-domain particles combined with surface and interface effects, size and structural inhomogeneities that cause broad ferromagnetic resonance.[49–51] These are frequently referred to as extrinsic damping mechanisms. With further optimization of the synthesis and processing to reduce the oxide shell thickness and increase the particle loading in the polymer and packing density, these problems could be addressed, leading to higher permeabilities and suppressed losses.

The high dielectric losses from dipole relaxation at 1 GHz to 5 GHz are also of concern with metal nanoparticle–polymer composites. The strategies for lowering this loss are not well understood, though literature indicates that the relaxation frequency can be shifted away from the operation frequency by varying the particle conductivity, size, and core–shell structures.[45]

Metal nanoparticles dispersed in the epoxy matrix thus show twofold enhancement in permittivity and permeability compared with traditional polymer dielectrics. This results in ~twofold reductions in antenna size. The losses are comparable to those of low-loss epoxies in the very high-frequency (VHF) and ultrahigh-frequency (UHF) range (~0.02, 100 MHz to 500 MHz), making them attractive for applications in this frequency range. A permeability of 2.5 and permittivity of 7.5 with a low magnetic loss of 0.02 in the VHF and UHF frequency range enable significant antenna size reduction with higher bandwidth than traditional RF dielectrics. These properties are superior to other metal nanocomposites[27] and ferrites[19,28] reported in the literature till 0.5 GHz. However, hexaferrites[18] and certain nanoscale anisotropic metal nanocomposite structures[38,40] are reported to have higher permeability and improved frequency stability above 1 GHz compared with the nanocomposites studied here. The degradation of properties in the current nanocomposites is attributed to the demagnetization and ferromagnetic resonance (FMR) broadening in the oxide-passivated nanoparticles. With further reduction in the oxide shell thickness and improved nanoparticle packing, higher permeability and lower losses can be retained at GHz frequencies. This will make them more suitable for a broader set of applications.

CONCLUSIONS

This paper describes a metal–polymer nanocomposite dielectric approach for high-frequency RF applications. The frequency-dependent magnetic properties were extracted by using an impedance analyzer. The metal nanocomposite structure showed both high permittivity and permeability and low losses in the VHF and UHF frequency range.

The GHz frequency-dependent material characteristics of the magnetodielectric films were extracted from corner-probing of parallel-plate resonators and strip inductors. Permeability of ~2 and permittivity of ~7.4 above 1 GHz frequency were demonstrated with the thin-film approach. Though eddy-current losses are suppressed in these systems, the high coercivity and resonance damping lead to high losses above 1 GHz. With further reduction in loss, the magnetic nanomaterials described herein could be applied to antenna and other RF components, leading to significant miniaturization and performance enhancement.

A process to integrate nanoscale metal composites at high loading onto organic substrates as thin-film build-up layers using standard packaging technologies such as screen-printing, mechanical via-drilling, and electroplating has also been demonstrated.

ACKNOWLEDGEMENTS

The authors wish to thank Intel Corporation for supporting this work.

REFERENCES

1. P.M. Raj, H. Sharma, D. Mishra, K.P. Murali, K. Han, M. Swaminathan, and R. Tummala, *IEEE Nanotechnol. Mag.* 6, 18 (2012).
2. M. Swaminathan, V. Sundaram, J. Papapolymerou, and P. Markondeya Raj, *IEEE Microw. Mag.* 12, 62 (2011).
3. G.-M. Yang, X. Xing, A. Daigle, M. Liu, O. Obi, J.W. Wang, K. Naishadham, and N.X. Sun, *IEEE Trans. Magn.* 44, 3091 (2008).
4. L.J. Martin, S. Ooi, D. Staiculescu, M.D. Hill, C.P. Wong, and M.M. Tentzeris, *IEEE Trans. Compon. Packag. Manuf. Technol.* 32, 849 (2009).
5. N. Altunyurt, M. Swaminathan, P.M. Raj, and V. Nair, *Proceedings of the 59th Electronic Components and Technology Conference*, vol. 801 (2009).
6. O. Dernovsek, A. Naeini, G. Preu, W. Wersing, M. Eberstein, and W.A. Schiller, *J. Eur. Ceram. Soc.* 21, 1693 (2001).
7. S. Ghosh, A. Hilgers, T. Schlenker, and R. Porath, *J. Eur. Ceram. Soc.* 21, 2621 (2001).
8. N. Altunyurt, R. Rieske, M. Swaminathan, and V. Sundaram, *IEEE Trans. Adv. Packag.* 32, 797 (2009).
9. G. Dejean, R. Bairavasubramanian, D. Thompson, G.E. Ponchak, M.M. Tentzeris, and J. Papapolymerou, *IEEE Antennas Wirel. Propag. Lett.* 4, 22 (2005).
10. H. Mossallaei and K. Sarabandi, *IEEE Trans. Antennas Propag.* 52, 1558 (2004).
11. Y. Liu, Y. Wang, and R. Yang, Proceedings of the 6th International Symposium on Antennas, Propagation and EM Theory, 2003, vol. 116 (2003).
12. K. Buell, H. Mosallaei, and K. Sarabandi, *IEEE Trans. Antennas Propag.* 54, 135 (2006).
13. P.B.A. Fechine, A. Távora, L.C. Kretly, A.F.L. Almeida, M.R.P. Santos, F.N.A. Freire, and A.S.B. Sombra, *J. Electron. Mater.* 35, 1848 (2006).
14. R.E. Collin, *Foundations for Microwave Engineering*, 2nd ed. (New York: McGraw-Hill, 1992), p. 450.
15. H. Bayrakdar, *J. Magn. Magn. Mater.* 323, 1882 (2011).
16. K.N. Rozanov, Z.W. Li, L.F. Chen, and M.Y. Koledintseva, *J. Appl. Phys.* 97, 013905 (2005).

17. L. Yang, L.J. Martin, D. Staiculescu, C.P. Wong, and M.M. Tentzeris, *IEEE Trans. Microw. Theory Tech.* 56, 3223 (2008).
18. J. Lee, Y.-K. Hong, S. Bae, J. Jalli, and G.S. Abo, *J. Appl. Phys.* 109, 07E530 (2011).
19. S. Bae, Y.K. Hong, J.J. Lee, J. Jalli, G.S. Abo, A. Lyle, I.T. Nam, W.M. Seong, J.S. Kum, and S.H. Park, *IEEE Trans. Magn.* 45, 2557 (2009).
20. F. Mazaleyrat and L.K. Varga, *J. Magn. Magn. Mater.* 215–216, 253 (2000).
21. S.B. Liao, *Ferromagnetic Physics* (Beijing: Science Press, 1992), p. 11.
22. P. Gramatyka, R. Nowosielski, P. Sakiewicz, and J. Achiev, *Mater. Manuf. Eng.* 20, 115 (2007).
23. R. Nowosielski and J. Achiev, *Mater. Manuf. Eng.* 24, 68 (2007).
24. A.H. Taghvaei, H. Shokrollahi, and K. Janghorban, *Mater. Des.* 31, 142 (2010).
25. A.H. Taghvaei, H. Shokrollahi, A. Ebrahimi, and K. Janghorban, *Mater. Chem. Phys.* 116, 247 (2009).
26. Y. Shirakata, N. Hidaka, M. Ishitsuka, A. Teramoto, and T. Ohmi, *IEEE Trans. Magn.* 40, 9 (2008).
27. W. Yang, L. Qiao, J. Wei, Z. Zhang, T. Wang, and F. Li, *J. Appl. Phys.* 107, 033913 (2010).
28. D. Guo, Z. Zhang, M. Lin, X. Fan, G. Chai, Y. Xu, and D. Xue, *J. Phys. D Appl. Phys.* 42, 125006 (2009).
29. Y. Hayakawa, A. Makino, H. Fujimori, and A. Inoue, *Jpn. J. Appl. Phys.* 81, 8 (1997).
30. S. Ohnuma, H. Fujimori, T. Masumoto, X.Y. Xiong, D.H. Ping, and K. Hono, *Appl. Phys. Lett.* 82, 946 (2003).
31. G. Herzer, *IEEE Trans. Magn.* 26, 1397 (1990).
32. G. Herzer, *Scripta Metall. Mater.* 33, 1741 (1995).
33. Y. Zhao, C. Ni, D. Kruczynski, X. Zhang, and J.Q. Xiao, *J. Phys. Chem. B* 108, 3691 (2004).
34. S. Ge, D. Yao, M. Yamaguchi, X. Yamg, H. Zuo, T. Ishii, D. Zhou, and F. Li, *J. Phys. D Appl. Phys.* 40, 3660 (2007).
35. N. Tang, W. Zhong, X. Wu, H. Jiang, W. Liu, and Y. Du, *Mater. Lett.* 59, 1723 (2005).
36. X. Ma, Y. Zhang, S. Ge, D. Zhang, D. Yan, and D. T. Xiao, US Patent, 7,485,366 B2 (2009).
37. K. Peng, L. Zhou, A. Hu, Y. Tang, and D. Li, *Mater. Chem. Phys.* 111, 34 (2008).
38. W. Liu, W. Zhong, H. Jiang, N. Tang, X. Wu, and Y. Du, *Surf. Coat. Technol.* 200, 5170 (2006).
39. Y.D. Zhang, S.H. Wang, D.T. Xiao, J.I. Budnick, and W.A. Hines, *IEEE Trans. Magn.* 37, 2275 (2001).
40. X. Kou, X. Fan, H. Zhu, R. Cao, and J.Q. Xiao, *IEEE Trans. Magn.* 46, 1143 (2010).
41. M. Darques, J. Spiegel, J. DelaTorr Medinaa, I. Huynen, and L. Piraux, *J. Magn. Magn. Mater.* 321, 2055 (2009).
42. B. Lu, X.L. Dong, H. Huang, X.F. Zhang, X.G. Zhu, J.P. Lei, and J.P. Sun, *J. Magn. Magn. Mater.* 320, 1106 (2008).
43. A. Bonincontro, C. Cametti, and A. Di Biasio, *J. Phys. D Appl. Phys.* 13, 1529 (1980).
44. G.M. Tsangaris, G.C. Psarras, and N. Kouloumbi, *Mater. Sci. Technol.* 12, 533 (1996).
45. I.J. Youngs, N. Bowler, K.P. Lymer, and S. Hussain, *J. Phys. D Appl. Phys.* 38, 188 (2005).
46. J.P. Chen, C.M. Sorensen, K.J. Klabunde, and G.C. Hadjipanayis, *Phys. Rev. B* 51, 11527 (1995).
47. V.B. Bregar, *IEEE Trans. Magn.* 40, 1679 (2004).
48. A.E. Berkowitz and K. Takano, *J. Magn. Magn. Mater.* 200–201, 552 (1999).
49. V. Castel, J.B. Youssef, and C. Brosseau, *J. Nanomater.* Article ID 27437 (2007).
50. R. Perzynski and Y.L. Raikher, *Surface Effects in Magnetic Nanoparticles*, ed. D.A. Fiorani (Ottawa: Nanostructured Science and Technology Series, 2005), p. 180.
51. Y.A. Koksharov, *Magnetic Nanoparticles*, ed. S.P. Gubin (Weinheim: Wiley-VCH, 2009), p. 231.